Low-cost, microcontroller-based, two-channel piezoelectric bender device for somatosensory experiments

Lucy Yan, *Student Member, IEEE*, and Luke E. Hallum, *Member, IEEE*

***Abstract*—Understanding the joint encoding of multiple tactile stimulus features (e.g., spatial position, amplitude, and frequency of vibration) is a major goal of somatosensory neuroscience, and the development of experimental set-ups to probe joint encoding is important. We describe in detail a microcontroller-based, piezoelectric bender device for tactile experiments. The device comprises an Arduino Due microcontroller board with a 32-bit ARM Cortex-M3 RISC processor, and two 12-bit digital-to-analog converters, enabling precise, independent stimulation of adjacent epithelial points. Using laser doppler vibrometry, we developed a model of the benders' structural mechanics, which we implemented on the device. We used the device to delivered precise, reliable somatosensory stimulation in an experimental setting, recording electrophysiological responses in the peripheral nervous system of the Gisborne cockroach (*Drymaplaneta semivitta*) to sinusoidal vibration of tibial spines. We plotted tuning curves and derived bandwidths of multi-unit populations. We also stimulated rat facial vibrissae *ex vivo*. This microcontroller-based, low-cost, open-source system leverages a large developer community associated with Arduino, and may help speed advances in systems neuroscience.**

I. Introduction

Our understanding of tactile somatosensory systems has been developed, traditionally, by measuring neural responses to stimulation of single points on sensory epithelia. Examples of this approach span a wide range of animal species (e.g., [1]-[3]). However, when an animal interacts with an object in its natural environment, that object rarely impresses upon only a single epithelial point. Rather, objects are spatially extended, meaning an animal's nervous system, in order to develop useful object representations that guide behaviour, must integrate signals that differ along many stimulus dimensions, including spatial position, stimulus amplitude, and vibration frequency. Understanding somatosensory systems' joint encoding of multiple stimulus features is a major goal of systems neuroscience, and the development of experimental set-ups to probe joint encoding is important.

There are few detailed, open-source descriptions of multi-channel tactile stimulation that are Arduino microcontroller-based. Sun & Okada [4] reported a microcontroller-based piezoelectric device to impress Braille on fingertips while measuring the magneto- and electroencephalogram. That device made use of the Arduino Uno's multiple digital outputs, a shift register, and a DC-to-DC converter to simultaneously activate dots comprising five Braille cells. Piezoelectric devices under the control of a desktop computer have been widely used in research concerning rodent whisker pathways (e.g., [5]). A noteworthy example is Jacob et al. [6], who reported a sophisticated 24-channel system controlled by a desktop computer, installed with two 32-channel PCI (peripheral component interconnect) cards for analog signal output.

Here, we provide a detailed, open-source description of an inexpensive Arduino Due microcontroller-based piezobender device for use in tactile experiments. We have validated the device in an animal model *(Drymaplaneta semivitta*).

II. Methods

A. Device description

Our device comprises the following key components connected in order: an Arduino Due microcontroller (Interaction Design Institute Ivrea, Ivrea, Italy); a pair of custom, low-pass filters; a pair of boost converters (PDm200B; PiezoDrive, Shortland, NSW, Australia); and two piezobenders (BA4902; PiezoDrive, Shortland, NSW, Australia) cantilevered in a custom bolt assembly (Fig. 1).

The Arduino Due microcontroller environment comprises two independent analog outputs, each able to produce a range of 2.2V with 12-bit resolution. We built two identical custom low-pass Butterworth filters to condition the Arduino Due's analog outputs. Each filter's cutoff was 160 Hz (3 dB down) with roll-off of -60 dB/decade. These filters were necessary to smooth the discretized sinusoidal waveform at high frequencies, and to attenuate transient artifacts that occasionally appeared on the Arduino Due's analog outputs. The boost converter had a gain of 20, so the maximum amplitude of the input to the piezobenders was 22 V. At

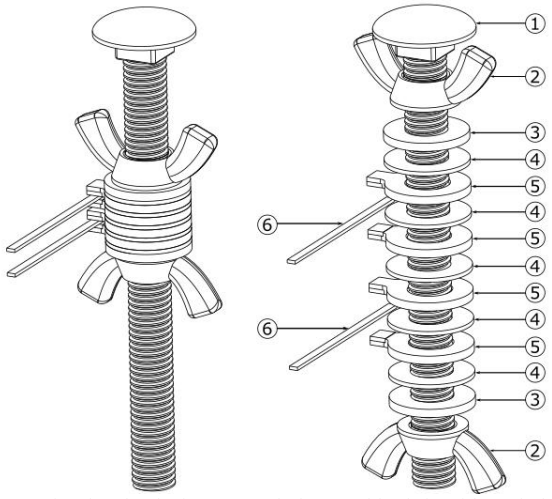

Figure 1. Piezobender device custom bolt assembly (left) with exploded view (right). The two benders, labeled ⑥, are held between pairs of tab washers (⑤) cut from 2 mm acrylic with 1mm thick rubber pads on the tabs. These are separated by 1 mm thick rubber washers (④). This assembly is then held together by stainless steel wingnuts and washers (② and ③ respectively) on an M10 stainless steel bolt (①).

L. Yan and L. Hallum are with the Dept. of Mechanical Engineering, University of Auckland, Auckland Central, New Zealand 1010 (email: lyan833@aucklanduni.ac.nz).

978-1-7281-1990-8/20/$31.00 ©2020 IEEE

moderate frequencies (e.g., between 10 and 150 Hz), this caused a peak-to-peak displacement of the bender tips of up to approximately 70 µm when the bender was clamped at 38 mm of free-standing length. The benders had dimensions of 49 x 2.1 x 0.8 mm with a mass of 0.4 g and stiffness of 100 N/m. To minimize mechanical crosstalk and to create separation between benders (e.g., to stimulate rodent facial vibrissae at greater separations), the tab washer pairs were isolated using 1 mm thick rubber washers. Tab washer pairs were secured using wingnuts and metal washers. Rubber washers and gaskets were laser-cut from 1 mm-thick rubber sheet (Field Rubber Ltd., Auckland, New Zealand).

B. Device characterization

We characterized our device by applying sinusoidal voltage inputs to a piezobender clamped at a free-standing length of 38 mm. We applied sine-wave and constant stimuli with stimulations amplitudes of 2.5, 5, 10, and 20 V. For each sine-wave stimulus, 10-second measurements were made at a range of frequencies between 1 and 420 Hz. Constant-valued stimuli were used as baseline control measurements. Velocity was measured using a laser doppler vibrometer (PDV-100; Polytec, Waldbronn, Germany) trained on the distal tip of the bender, and displacement waveforms were derived using fast Fourier transforms. We compared results from our device to those of an ideal system in which a wave generator (InfiniiVision DSOX2002A; Keysight Technologies, Santa Rosa, CA) and ideal amplifier (EPA-104; Piezo Systems, Woburn, MA 01801 United States) replaced our Arduino Due, custom low-pass filter, and boost converter.

We modeled the frequency response function (FRF) of our device, fitting equations (1) and (2) to derived displacement amplitudes and phases of the bender using ordinary least-squares [7]. Displacement was fit using the following equation:

$$x_0 = \frac{P_0}{k \times \sqrt{\left(1-\frac{f^2}{f_n^2}\right)^2 + \left(2\frac{c}{c_c}\times\frac{f}{f_n}\right)^2}} \quad (1)$$

where x_0 is the maximum amplitude of displacement, P_0 is the nominal force applied to the system, k is the stiffness constant, f are the frequencies at which the displacements are calculated, f_n is the natural frequency of the piezobender, c is the damping constant, and c_c is the critical damping constant. Phase was fit using the following equation:

$$\phi = \operatorname{atan}\left(\frac{2\frac{c}{c_c}\times\frac{f}{f_n}}{1-\frac{f^2}{f_n^2}}\right) \quad (2)$$

where ϕ is the phase of the displacement of the system and all other terms are as in equation (1).

We quantified our device's linearity by computing a linearity index (LI) as the ratio of the derived displacement amplitude at the drive frequency to the sum of the displacement amplitudes at the drive frequency and its first and second harmonics. LI could range from 0 to 1; values near unity indicated the displacement waveform was sinusoidal.

We used equation (1) to linearize the displacement of our device such that we were able to apply constant-amplitude stimulation to biological preparations at a wide range of biologically relevant frequencies.

C. Device validation

We studied the electrophysiological effect of our device on *D. semivitta*. The animal was decapitated and a metathoracic leg amputated before mounting on putty. Experiments typically lasted 1 hour. We gained electrical access to neuropil by inserting 0.4 mm-diameter stainless steel insect pins (Conservation Supplies, Havelock North, Hastings, New Zealand) through the carapace; one in the coxa (reference electrode), and the other in the femur in the vicinity of the femoral nerve (active electrode). We then determined the most responsive tibial spine by hand. For control measurements, the bender, close to but not touching the spine, was driven at constant displacement amplitude at a range of frequencies, each separated from the next by one octave (1, 2, 4, … 256 Hz). At each frequency, continuous 30-second recordings were made of the electrophysiological response and bender velocity. Because *D. semivitta*'s tibial spines are extremely sensitive to vibration, we clamped the bender at a shorter free-standing length (20 mm) and used smaller driving displacements. The 20 mm free-standing length increased the first resonant frequency to approximately 600 Hz, so we reconfigured our low-pass filter (cutoff = 300 Hz) to allow higher-amplitude stimulation at moderate-to-high frequencies. The tip of the piezobender was then superglued to the caudal face of that spine such that the bender oscillated the spine in the rostrocaudal direction, and the same recordings were made. Raw recordings were band-pass filtered (cutoffs = 600, 6000 Hz) offline to recover multi-unit spikes. Multi-unit responses were estimated by using threshold crossings selected by eye on an animal-by-animal basis to form a time series of impulses. The modulated response of the tibial spine was calculated as the amplitude of the Fourier component of these impulses at each stimulus frequency, used, for example, by Cloherty and Ibbotson [8].

At each frequency, we estimated the modulated response to stimulation in units of spikes per second. We used weighted least-squares to fit a double exponential, commonly used to model visual contrast sensitivity (e.g., [9]), to mean or modulated responses:

$$s(f) = a \times f^b \exp(-cf) \quad (3)$$

where s is the neural response, f are the frequencies of stimulation, and $a, b,$ and c are free parameters.

III. Results

A. Device characterization

Our device delivered sinusoidal vibrations within a wide range of biologically relevant frequencies (1 to 420 Hz). At very low frequencies (< 1 Hz), bender velocity measurements were contaminated by noise. This is a consequence of the dynamic range of our vibrometer, not the fidelity of the signal generated by our device; when benders were driven at very low frequencies by the ideal system (Methods), their velocities were similarly affected. At very high frequencies (> 265 Hz), Arduino Due-driven vibrations were less sinusoidal. This distortion was a limitation of the DAC in the Arduino Due; by comparison, when benders were driven at very high frequencies by the ideal system, responses did not deteriorate. For frequencies between 1 and 265 Hz, the

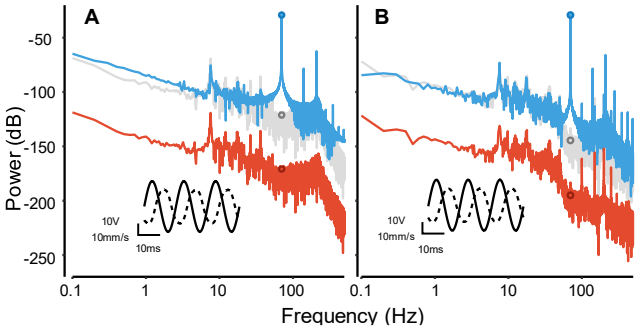

Figure 2. Example recordings and power spectra of piezobender tip in characterization of our device. (A) The inset shows a 70 Hz driving sine wave (solid line) generated by our device and input to a clamped piezobender. Using laser vibrometry, we measured the velocity of the bender's distal tip (dashed). We show the spectrum of the derived tip displacement (blue). Peak-to-peak displacement at 70 Hz = 67.0 µm. We also show the baseline (constant voltage) spectrum (gray), shifted -50 dB for clarity (red). For each trace, the power at 70 Hz is circled. (B) As in A but, for comparison, ideal voltage source and amplifier. Peak-to-peak displacement at 70 Hz = 67.9 µm.

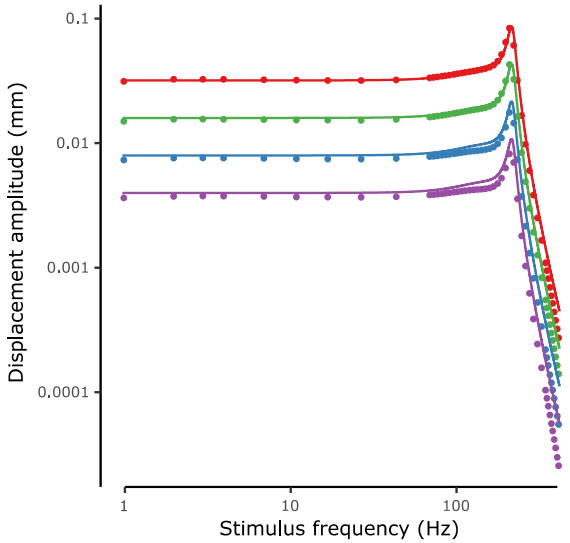

Figure 3. Characterization of piezobender tip displacement versus stimulus frequency for sinusoidal inputs at 2.5 (purple), 5 (blue), 10 (green), and 20 V (red). Solid lines show model fit; modeled 1st resonant frequency = 216 Hz. The fits differ only by a vertical shift, indicative of the linear relationship between driving voltage and displacement. Phase response (not shown) was similar at all driving voltages and revealed a reversal at 216 Hz, characteristic of resonance.

sinusoidal vibrations produced by the Arduino Due were high-fidelity. The example power spectra in Fig. 2 show that most of the power of the vibration of the bender is at the drive frequency when driven both by our device and by the ideal system. All other frequencies have little power. The calculated LI value indicated that the bender's sinusoidal displacements were high-fidelity; for our device, LI was greater than 0.96 for all frequencies tested (1 to 420 Hz). By comparison, for the ideal system, LI was greater than 0.98 across all frequencies from 1 to 420 Hz. We measured negligible mechanical crosstalk between piezobenders; at most, crosstalk amplitude was on the order of 0.1 µm.

We estimated the FRF of a piezobender using our device and compared that estimate to the FRF of an ideally-driven bender. We derived displacement amplitude of the bender's distal tip when driven at 20 V amplitude by our device (plotted in red in Fig. 3) and the ideal source (not plotted) at frequencies spanning a wide, biologically relevant range. At frequencies much lower than the bender's first resonant frequency (i.e., between 1 and 70 Hz), the displacement amplitude was approximately constant at 80 µm when driven by either the Arduino Due or the ideal source. Displacement amplitude increased near the bender's first resonant frequency, and rapidly decreased thereafter. At frequencies above 70 Hz, the Arduino Due-driven bender had smaller amplitudes than the ideally-driven bender; this difference was largely due to the attenuation caused by our low-pass filter and poor signal quality at high frequencies. The parameters of the models used to formulate the FRFs include those in equations (1) and (2), as well as the propagation delay of the laser vibrometer, and parameters describing a low-pass filter. This filter characterizes the attenuation in displacement that occurs at higher driving frequencies of the bender.

We also assessed the linearity of our device by applying sinusoids at a range of octave-spaced input voltage amplitudes (2.5, 5.0, 10.0, 20.0 V), at the same frequencies between 1 and 420 Hz. In Fig. 3 we plot the amplitudes of the FRFs on log-log axes for these input voltages; the near-equal vertical shifts of otherwise similar displacement amplitude functions on log-log axes are characteristic of linearity. We simultaneously fit four FRFs to these data using equation (1), each being a scalar multiple of a base FRF where the input voltage amplitude was 1 V. The scalar multiplier for each of the four FRFs is equal to the voltage amplitude being applied. All other parameters were shared between the four FRFs.

B. Device validation

We validated our linearized device by actuating tibial spines of *D. semivitta* and observing the response selectivity to frequency, i.e., the modulated response. We did so by gluing the distal tip of the bender to a tibial spine and driving it sinusoidally at a range of frequencies while measuring both the afferent fibre activity in the femoral nerve (Fig. 4A) and the velocity of the distal tip of the piezobender. Because *D. semivitta*'s tibial spines are very sensitive to vibration, we applied only small-amplitude displacements. These small vibrations were effective in eliciting vigorous responses from afferent fibres, as illustrated by the example recording in Fig. 4A. In one cockroach, responses were most vigorous in the band between 2 and 16 Hz, and the fitted modulated multi-unit responses were maximum at 6.93 Hz (Fig. 4B). The modulated spiking response from the same experiment repeated on a different cockroach also showed bandpass behaviour, though in a different range; responses were most vigorous between 8 and 64 Hz, with the optimal stimulus frequency being 26.11 Hz (Fig. 4C). The relative increase in response rate shown in Fig. 4 is likely to have resulted from a blend of electrode proximity to the responding nerves and an increase in the displacement amplitude of the bender. The examples shown in Fig. 4 are representative of our recordings in many animals. Across nine such recordings, the fitted descriptive models (Methods) revealed average peak modulated response rates at a stimulus frequency of 18.2 ± 12.28 Hz, with bandwidths (full-width at half-maximum) of 4.32 ± 1.19 octaves. Recordings that had poor interaction between the piezobender and the cockroach spine were excluded.

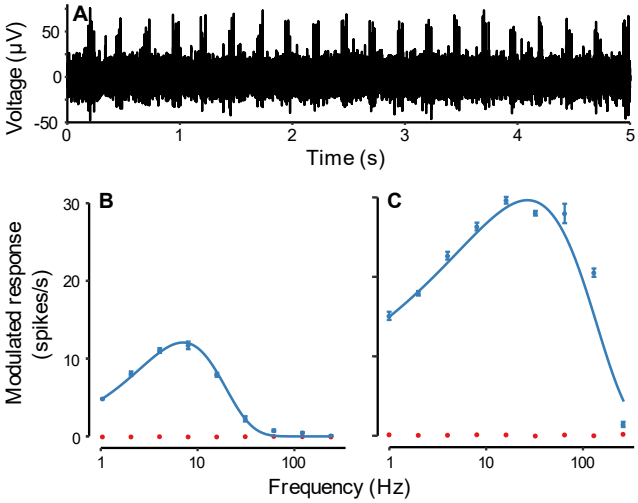

Figure 4. Device validation. We measured responses to stimulation of tibial spines in *D. semivitta*'s femoral nerve. (A) Example recording showing multi-unit response modulation at the stimulus frequency (4 Hz). (B) Tuning curve for the units in A. The fitted double exponential function (blue) was used to derive tuning bandwidth. Error bars, standard error. Red symbols, control measurements. (C) As in B, but different animal.

IV. Discussion

We have provided a detailed description of an inexpensive, Arduino Due microcontroller-based piezobender device for use in somatosensory experiments. The Due's two 12-bit digital-to-analog converters (DACs) enable precise, independent stimulation of adjacent points on the somatosensory epithelium at a range of biologically relevant amplitudes and frequencies, and with little crosstalk. We implemented on the device a model of the deflection of benders rooted in cantilevered beam theory. We validated the linearized device in the peripheral nervous system of *D. semivitta*.

Our device characterization revealed high-fidelity sinusoidal stimulation between frequencies of 1 and 265 Hz. This range likely encompasses frequencies that *D. semivitta* encounters in its natural environment. To our knowledge, there are no other reports of measurements or analyses of the frequency response function of tactile spines in this species. There are several early studies of the American cockroach (*Periplaneta americana*); many of those studies applied only low-frequency vibrations, presumably limited by hardware (e.g., [10]). French and Kuster [11] made measurements similar to ours in *P. americana*, stimulating a single spine with broadband vibration (up to 500 Hz). They calculated the coherence between the applied vibration and the rate of action potential firing. Coherence is a function of frequency which ranges between 0 and 1, where 1 indicates that the FRF completely characterizes the system at that frequency, and is a measure comparable to ours of modulated response. French and Kuster found coherence to be bandpass in nature, peaking between 20 and 70 Hz. Similarly, the modulated responses in *D. semivitta* tended to be bandpass, typically greatest between 8 and 64 Hz. Our results suggest that the frequency response functions of the tactile spines of *D. semivitta* are similar to those of *P. americana*.

Piezobenders are not uncommon in tactile physiological and psychophysical experiments (e.g., [12]). When used in that setting, benders are often assumed to be well behaved; that is, to deliver stimuli with no distortion arising from either resonance or mechanical resistance encountered at the sensory epithelium. Here, we quantified distortion, measuring fidelity of the sinusoidal displacement of the bender, and attenuation of the applied displacement, in both loaded and unloaded conditions. In some cases, we found appreciable distortion of up to 24%, even for light loads such as the tibial spine of a cockroach. Additional measurements using the benders on rat facial vibrissae trimmed to 10 mm in length (here, not reported) showed negligible distortion (< 2%). Homma and colleagues [13] applied piezoelectric pins to the human fingertip, and developed a model of fingertip resistance to stimulation. In future work, a model like theirs, adapted to the mechanics of a cockroach's tibial spine, could be integrated with our mechanical model to further improve the linearity of our device.

Acknowledgments

We thank Matt Carleton, Marshall Lim, and Emanuele Romanò for technical support.

References

[1] V. B. Mountcastle, M. A. Steinmetz, and R. Romo, "Frequency discrimination in the sense of flutter: Psychophysical measurements correlated with postcentral events in behaving monkeys," *J. Neurosci.*, vol. 10, no. 9, pp. 3032–3044, 1990.

[2] A. B. Vallbo and R. S. Johansson, "Properties of cutaneous mechanoreceptors in the human hand related to touch sensation," *Hum. Neurobiol.*, vol. 3, no. 1, pp. 3–14, 1984.

[3] J. A. Burdohan and C. M. Comer, "Cellular organization of an antennal mechanosensory pathway in the cockroach, Periplaneta americana," *J. Neurosci*., vol. 16, no. 18, pp. 5830–5843, 1996.

[4] L. Sun and Y. Okada, "Vibrotactile piezoelectric stimulation system with precise and versatile timing control for somatosensory research," *J. Neurosci. Methods*, vol. 317, no. February, pp. 29–36, 2019.

[5] P. J. Drew and D. E. Feldman, "Representation of moving wavefronts of whisker deflection in rat somatosensory cortex," *J. Neurophysiol.*, vol. 98, no. 3, pp. 1566–1580, 2007.

[6] V. Jacob et al., "The Matrix: A new tool for probing the whisker-to-barrel system with natural stimuli," *J. Neurosci. Methods*, vol. 189, no. 1, pp. 65–74, 2010.

[7] J. P. Den Hartog, *Mechanical vibrations*. New York: Dover Publications, 1985.

[8] S. L. Cloherty and M. R. Ibbotson, "Contrast-dependent phase sensitivity in V1 but not V2 of macaque visual cortex," *J. Neurophysiol.*, vol. 113, no. 2, pp. 434–444, 2015.

[9] C. Shooner *et al.*, "Population representation of visual information in areas V1 and V2 of amblyopic macaques," *Vision Res.*, vol. 114, pp. 56–67, 2015.

[10] B. Y. J. W. S. Pringle and V. J. Wilson, "The Response Of A Sense Organ To A Harmonic Stimulus," *J. Exp. Biol.*, vol. 29, no. 2, pp. 220–234, 1952.

[11] A. S. French and J. E. Kuster, "Sensory Transduction in an Insect Mechanoreceptor: Extended Bandwidth Measurements and Sensitivity to Stimulus Strength," *Biol. Cybern.*, no. 42, pp. 87–94, 1981.

[12] M. R. Bale et al., "Learning and recognition of tactile temporal sequences by mice and humans," *Elife*, vol. 6, pp. 1–21, 2017.

[13] T. Homma, S. Ino, H. Kuroki, T. Izumi, and T. Ifukube, "Development of a piezoelectric actuator for presentation of various tactile stimulation patterns to fingerpad skin," *Annu. Int. Conf. IEEE Eng. Med. Biol.*, vol. 26 VII, pp. 4960–4963, 2004.